CrossMark

# An Episode of Occultation Events in Gaia21bcv

Klaus W. Hodapp[1] , Eric Gaidos[2] , Matthew A. Kenworthy[3] , Michael Tucker[4,5,8] , Benjamin J. Shappee[6] ,
Anna V. Payne[6,7] , and Aaron Do[6]
[1] University of Hawaii, Institute for Astronomy, 640 N. Aohoku Place, Hilo, HI 96720, USA; hodapp@ifa.hawaii.edu
[2] Department of Earth Sciences, University of Hawai'i at Mänoa, Honolulu, HI 96822, USA
[3] Leiden Observatory, Leiden University, P.O. Box 9513, 2300 RA Leiden, The Netherlands
[4] Center for Cosmology and Astroparticle Physics, The Ohio State University, 191 West Woodruff Avenue, Columbus, OH 43210, USA
[5] Department of Astronomy, The Ohio State University, 140 West 18th Avenue, Columbus, OH 43210, USA
[6] University of Hawaii, Institute for Astronomy, 2680 Woodlawn Drive, Honolulu, HI 96822, USA
[7] Space Telescope Science Institute, 3700 San Martin Drive, Baltimore, MD 21218, USA

## Abstract

A previously unremarkable star near the Canis Major OB1/R1 association underwent an episode of multiple deep brightness minima. Light curves based on archival Gaia, Zwicky Transient Facility (ZTF), and NEOWISE data and additional observations from the Las Cumbres Observatory and UKIRT show that the star was not variable prior to 2019 August 18 (MJD 58700), and on that date started showing brightness dips of up to 3 mag in the Gaia $G$ and ZTF $r$ bandpasses. After MJD 59500, ≈800 days after the onset of these dipping events, the star returned to its previous brightness, and no significant dipping events have been recorded since. Compared to the stable phase, NEOWISE IR photometry in the W1 and W2 bands indicates a generally redder color, and both decreases and increases in brightness at different times during the dipping episode. The spectrum of Gaia21bcv taken after the end of the dipping episode shows several neutral and ionized metal absorption lines, including Li, indicating a spectral type of ≈K5. Variable emission from [O I] was observed. The Hα absorption in Gaia21bcv is too faint and irregular for this spectral type, indicating that the line is partly filled in by variable emission, a signature of weak episodic accretion. Gaia21bcv lies above the zero-age main sequence, but is much fainter than typical R CrB stars. We interpret the light curve of Gaia21bcv as being similar to the occultation events in $\epsilon$ Aurigae, i.e., occultation by a disk around a companion object orbiting the primary star.

Unified Astronomy Thesaurus concepts: Pre-main sequence stars (1290); Debris disks (363); Occulting disks (1149); Transits (1711)

## 1. Introduction

Most young stars are variable, and variability is one of the characteristics used by Herbig (1962) to define the class of T Tauri stars. In addition to the variability caused by the modulation of star spots and instabilities in mass accretion onto the star, dipping events in young stars, i.e., multiple, often quasiperiodic minima, are due to occultation by dust condensations in the disks surrounding them, leading to the definition of the UXOr class of young variables by Herbst et al. (1994). A summary of the current understanding of dipper objects has recently been published by Roggero et al. (2021).

In contrast to the dipper phenomenon caused by density inhomogeneities in a circumstellar disk, where dips are continually occurring, a small class of variable stars show isolated episodes of deep minima lasting for months to years, separated by long phases of constant brightness. In those cases, the obscuring material must be confined to a small section of its orbit around the star, and these light curves have been interpreted as eclipsing events by a disk surrounding a companion object.

The prototypical object for such substantial periodic occultation events is $\epsilon$ Aurigae, where the brightness minima are caused by an optically thick circumstellar disk around a

companion star transiting the primary star, leading to periodic eclipses every 27.1 yr (Hoard et al. 2010). Similarly, KH15D, discovered by Kearns & Herbst (1998), has in recent decades started showing deep, quasiperiodic minima that increased in depth and duration, so that the star no longer reaches the unobscured light level between minima. The case of the eclipse of 1SWASP J1407, characterized by rapid variations during the occultation event, was discussed by Kenworthy & Mamajek (2015) and interpreted as being caused by a giant ring system around an unobserved object that itself orbits the star. This scenario of eclipsing disks in general has been discussed by Mamajek et al. (2012), who concluded that in a sample of 10,000 post-accretion stars monitored over 10 yr, several such eclipsing events would be predicted. The Gaia satellite observes any given point in the sky every few months (Gaia Collaboration et al. 2016) and the Gaia Alerts project[9] publishes unusual photometric behavior discovered in these repeated observations. The discovery of Gaia21bcv in the CMa OB1/R1 association of young stars, as a result of Gaia monitoring, is confirming the prediction by Mamajek et al. (2012) that more such secondary disk or ring occultation events remain to be discovered.

It should be noted that another class of variable star with similar long-duration drops in brightness are the R Coronae Borealis (RCB) stars—carbon-rich, post-main-sequence stars where the condensation of dust clouds is responsible for the dimming of the star. RCB stars are high-luminosity objects in

---

[8] CCAPP Fellow.

[9] http://gsaweb.ast.cam.ac.uk/alerts

the late phases of stellar evolution and can be distinguished from other dimming events, such as UXOrs, on this basis.

This paper reports the results of a photometric and spectroscopic observing campaign and the analysis of various archival records initiated after the Gaia21bcv alert.

## 2. Observations and Results

### 2.1. Photometry

#### 2.1.1. Gaia

Gaia21bcv was an unremarkable star of constant brightness in all the prior years for which photometry exists. Between 2015 and mid-2019, Gaia photometry of this star showed little variation, with a magnitude of $G = 17.70 \pm 0.03$. On 2019 August 18 (MJD 58713), Gaia recorded the star at $G = 20.12$, followed by a rapid rebrightening to $\approx G = 18.6$, when Gaia obtained the next light-curve data points on 2019 August 31. The minimum that triggered the Gaia alert on 2021 March 1 (MJD 59457) was actually the third major brightness minimum in the recent episode and was followed immediately by a rebrightening before the object seasonally became unobservable. The first few observations of the observing campaign in late 2021, when Gaia21bcv became observable again, recorded the end of another minimum. After MJD 59520 (2021 November 2), the object returned to its bright state and no further occultation events were observed. The Gaia satellite observes any given point in the sky every few months (Gaia Collaboration et al. 2016), sampling the rapid dipping events sparsely, but with greater precision than the available ground-based photometry.

#### 2.1.2. Zwicky Transient Facility

To complement the Gaia light-curve data, we have downloaded[10] archival $r$-band photometry of Gaia21bcv from the Zwicky Transient Facility (ZTF; Bellm et al. 2019) archive (Masci et al. 2019). We shifted all ZTF magnitudes by a fixed amount ($-0.1$ mag) to match the Gaia $G$ photometry.

#### 2.1.3. NEOWISE

At the position of Gaia21bcv, the NEOWISE mission (Mainzer et al. 2014) continues to obtain multiple photometric measurements over about a day, every six months. For the light curve in Figure 1, we have median combined all individual measurements from the WISE Team (2020) in each of these day-long intervals into one measurement. These combined photometric points and the resulting colors are listed in Table 1.

#### 2.1.4. UKIRT/WFCAM

We have monitored Gaia21bcv in the $z$, $J$, $H$, and K bands using WFCAM (Casali et al. 2007) on UKIRT. These observations started just when the eclipsing episode was coming to an end and only the first 40 days of this observing campaign contain information about the absorbing material. After that, the data only confirm that post-eclipse Gaia21bcv has returned to the same brightness as its Two Micron All Sky Survey (2MASS; Skrutskie 2006) catalog entry.
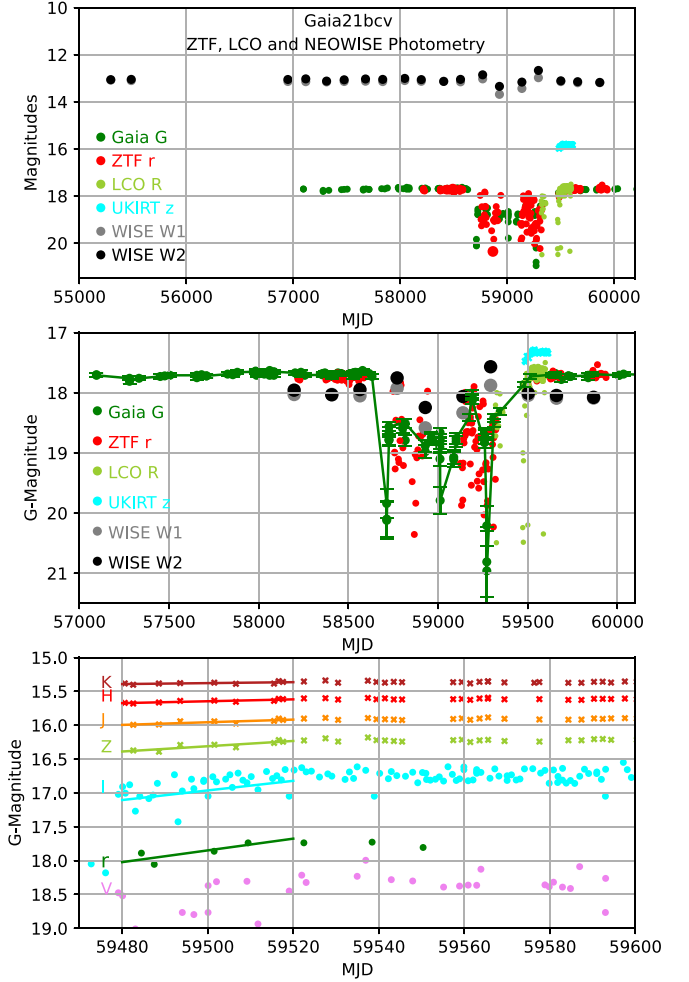
**Figure 1.** Gaia, ZTF, LCO, and NEOWISE light curve. The ZTF (red) data were shifted by 0.1 mag to match the Gaia $G$ photometry in the stable bright phase. Similarly, the LCO data were calibrated against Gaia $G$ in the bright phase. The errors of the Gaia $G$ photometry are shown, but in the bright phase are smaller than the symbols used. The errors in the ZTF photometry are not shown, to preserve some clarity of the figure, but are similar to those of the Gaia data. The errors of the NEOWISE data are not shown in the figure, but are listed in Table 1. The star was essentially constant prior to MJD 58600, after which time several deep dipping events were observed. After MJD 59500, these dipping events have ceased and the star has returned to near-constant brightness. The top panel gives the overview of the light curve, emphasizing the long time of constant brightness before the dipping episode. The center panel shows details of the dipping episode, with the NEOWISE IR data shifted by 4.9 mag for clarity. The bottom panel shows the details of the last month of the dipping episode and the return to stable brightness. LCO, ZTF, and UKIRT high-cadence photometry is shown, shifted in magnitude for clarity. The first month of the data shown here captured the last of the dipping events and the return to stable brightness. The magnitudes in that last month are fitted by a line to measure the extinction in different filters. The noise in the LCO data is substantially higher than in the IR UKIRT data, due to the fact that the LCO 1 m telescope is much smaller than the 3.8 m UKIRT, and the star is obscured by interstellar extinction and therefore faint at optical wavelengths.

#### 2.1.5. Las Cumbres Observatory

Gaia21bcv was observed over a span of 94 days between MJD 59496.8 and 59591.0 with the 1 m telescope network of the Las Cumbres Observatory Global Telescope (LCOGT; Brown et al. 2013). Photometry was obtained in Bessell $V$, $R$, and $I$ filters, with exposure times of 460, 80, and 50 s, respectively. The image processing and extraction of instrumental magnitudes were automatically performed using the LCOGT BANZAI pipeline (McCully et al. 2018), while the

**Table 1**
Gaia21bcv NEOWISE Photometry

| Epoch (MJD) | W1 (mag) | W2 (mag) | W1–W2 (mag) |
|---|---|---|---|
| 55292 | $-0.05 \pm 0.03$ | $-0.02 \pm 0.05$ | $0.02 \pm 0.06$ |
| 55484 | $-0.04 \pm 0.03$ | $-0.03 \pm 0.05$ | $0.05 \pm 0.06$ |
| 56949 | $0.00 \pm 0.03$ | $-0.02 \pm 0.05$ | $0.08 \pm 0.06$ |
| 57116 | $0.01 \pm 0.03$ | $-0.05 \pm 0.05$ | $0.12 \pm 0.06$ |
| 57311 | $0.02 \pm 0.03$ | $0.05 \pm 0.05$ | $0.04 \pm 0.06$ |
| 57476 | $0.00 \pm 0.03$ | $-0.01 \pm 0.05$ | $0.07 \pm 0.06$ |
| 57675 | $-0.01 \pm 0.03$ | $-0.04 \pm 0.05$ | $0.10 \pm 0.06$ |
| 57836 | $0.01 \pm 0.03$ | $-0.03 \pm 0.05$ | $0.09 \pm 0.06$ |
| 58042 | $-0.04 \pm 0.03$ | $-0.07 \pm 0.05$ | $0.09 \pm 0.06$ |
| 58196 | $-0.01 \pm 0.03$ | $-0.02 \pm 0.05$ | $0.07 \pm 0.06$ |
| 58406 | $-0.01 \pm 0.03$ | $0.06 \pm 0.05$ | $-0.01 \pm 0.06$ |
| 58564 | $0.02 \pm 0.03$ | $-0.03 \pm 0.05$ | $0.10 \pm 0.06$ |
| 58771 | $-0.11 \pm 0.03$ | $-0.22 \pm 0.05$ | $0.17 \pm 0.06$ |
| 58928 | $0.55 \pm 0.03$ | $0.27 \pm 0.05$ | $0.34 \pm 0.06$ |
| 59138 | $0.30 \pm 0.03$ | $0.09 \pm 0.05$ | $0.27 \pm 0.06$ |
| 59292 | $-0.16 \pm 0.03$ | $-0.41 \pm 0.05$ | $0.31 \pm 0.06$ |
| 59502 | $0.01 \pm 0.03$ | $0.03 \pm 0.05$ | $0.03 \pm 0.06$ |
| 59659 | $0.06 \pm 0.03$ | $0.07 \pm 0.05$ | $0.04 \pm 0.06$ |
| 59866 | $0.05 \pm 0.03$ | $0.10 \pm 0.05$ | $0.01 \pm 0.06$ |

determination of relative magnitudes corrected for individual image zero-points was carried out by custom software routines (Gaidos et al. 2022). This monitoring started a few weeks earlier than the other monitoring campaigns, at the beginning of the visibility period, and the first few data points recorded the last few days of the last dimming event.

### 2.1.6. Historic Photometry

Prior to the Gaia and WISE/NEOWISE missions, there are only a few photometric data points available in various surveys. The Pan-STARRS1 (PS1) database (Flewelling et al. 2020) photometry of rPSFMag = 17.92 from MJD 56888 (2014 August 19) is consistent with the brightness of Gaia21bcv outside of the dipping episode, considering the differences in the filter bandpasses. In the IR, data taken with more consistent filters are available.

The 2MASS magnitudes of Gaia21bcv in the stable bright phase are $J = 14.528$, $H = 13.676$, and $K_s = 13.338$ (on MJD 50904 = 1998 April 1), and the UKIDSS ($K = 13.37$ on MJD 55565 = 2011 January 4; Lawrence et al. 2007) near-IR data points are consistent with stable brightness. The UKIRT WFCAM photometry after the end of the dipping episode is $J = 14.52$, $H = 13.723$, and $K = 13.359$. This is very close to the 2MASS brightness transformed to the UKIRT WFCAM system via the equations in Hodgkin et al. (2009) of $J = 14.4726$, $H = 13.7356$, and $K = 13.350$. Within the uncertainties of these measurements, the brightness after the dipping episode is indistinguishable from that before it.

## 2.2. Optical Spectroscopy

### 2.2.1. UH88 Telescope and Super Nova Integral Field Spectrograph

We obtained optical spectra of Gaia21bcv at nine epochs between MJD 59502 (2021 October 14) and MJD 59663 (2022 March 25) using the Super Nova Integral Field Spectrograph (SNIFS; Wood-Vasey 2004) at the UH 88″ telescope through the SCAT survey (Tucker et al. 2022). The earliest of these observations just recorded the last few days of the last poorly observed minimum in the LCOGT and UKIRT photometry.

The other eight spectra were obtained when the object had returned to stable brightness. After MJD 59653, well into the stable bright phase, emission in the [O I] doublet at 6300 and 6364 Å was observed, while it was not seen prior to that time. To improve the signal-to-noise ratio over that of the individual exposures, we separately averaged all spectra with and without the [O I] line for Figure 3.

### 2.2.2. Keck I/HIRES

We obtained a high-resolution spectrum of Gaia21bcv on MJD 59617 and 59618 (2022 February 6 and 7), just after the apparent end of the dipping episode, with the Keck HIRES spectrograph (Vogt et al. 1994). We used a fairly narrow slit of 0″.6 to achieve a spectral resolution of ≈60,000 and used the longest slit possible to search for emission lines near the star and detected Hα and [S II] emission. The wavelength calibration used a combination of Th-Ar calibration spectra and telluric OH airglow lines, and Na I and Hα emission in the science data. The sky and extended background were measured along the slit, away from the point-source point-spread function. The comparison of telluric Na I night sky emission and the Na I absorption in the star gave a spectral shift of 0.828 Å, corresponding to a $31 \pm 1$ km s$^{-1}$ radial velocity relative to the solar system barycenter. Spectra extracted on source without sky subtraction are shown as the blue lines in Figure 4, while sky-subtracted spectra are shown in red.

## 3. Data Analysis and Results

### 3.1. Location and Distance

Gaia21bcv at coordinates $108°.63865 - 12°.22426$ (J2000.0) is listed in the Gaia Early Data Release 3 (EDR3) catalog (Gaia Collaboration et al. 2023) as object number 3045209156636885760, with a parallax of $0.72 \pm 0.13$ mas and renormalized unit weight error (RUWE) of 1.06, giving a distance of 1382 pc (1178–1672 pc) and distance modulus of 10.70 mag. Gaia21bcv (the cyan circle in Figure 2) appears to lie on the southeastern edge of a region of reduced star density on DSS red and blue, identified as the dark nebula DOBASHI5098 (Dobashi 2011). The PS1/UKIRT gJK color composite image in Figure 2 shows a large number of very red objects in the area of the dark cloud, which also contains a mid-IR source, WISE J071429.04-121239.5, indicated by the yellow circle in Figure 2.

Gregorio-Hetem et al. (2021) have studied young stars in the Canis Major OB1/R1 OB association that forms a ringlike system of molecular clouds, with the brightest optically visible object being the H II region $Sh2 - 296$ near the western edge of the association. They concluded, based on its parallax and proper motion, that Gaia21bcv is a Class III object, with a probability of membership in the OB association of 85%. Numerous Hα-emitting young stars have been found in the CMa OB1/R1 region by Pettersson & Reipurth (2019), including the area immediately surrounding Gaia21bcv, but Gaia21bcv was not included in their list of Hα stars.

Using Gaia DR2 data, Santos-Silva et al. (2021) identified groups of stars in CMa OB1/R1 based on their position and proper motion. Gaia21bcv lies outside these defined groups and therefore was not assigned an age. A small grouping of bright, blueish stars is just west of Gaia21bcv. The brightest of these is HD 55902 ($V = 8.7$), a B9III star with low extinction and a
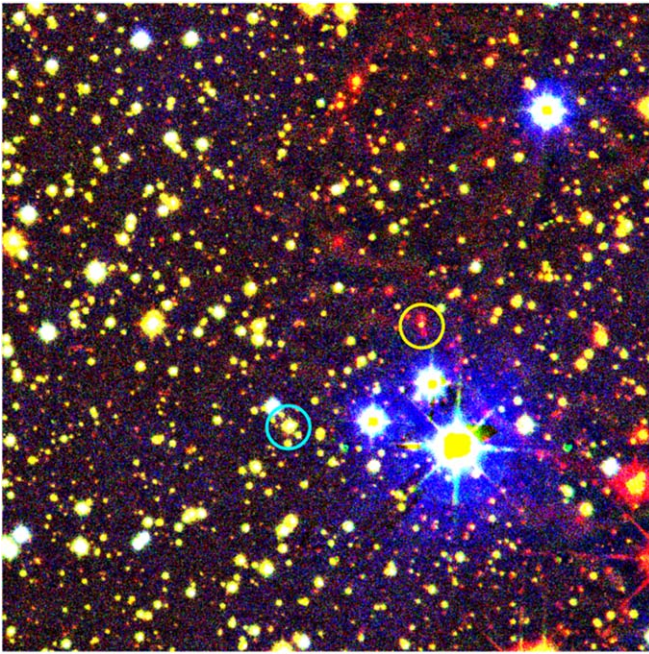
**Figure 2.** *gJK* color composite image of the 5′ × 5′ region near Gaia21bcv, showing extended emission in the red image and evidence of absorption. Gaia21bcv is marked by the cyan circle. The yellow circle indicates the position of the embedded IR source WISE J071429.04-121239.5.

parallax of 1.52 mas, $d = 656$ pc. These bright stars are in the foreground of Gaia21bcv and not physically close to it.

The Keck HIRES spectrum detected H$\alpha$ emission both from telluric emission (the narrow emission line) and from the nebulosity near Gaia21bcv (the broadline component). Fitting a Gaussian function to the broadline profile gives a barycentric radial velocity of $27 \pm 11$ km s$^{-1}$.

### 3.2. Properties of the Star

#### 3.2.1. Spectral Type

The combined SNIFS spectra show a continuum slope that in itself would match the continuum slope of a mid-M spectral type. However, such a late type can be excluded, since we do not observe the deep molecular absorption features, primarily of TiO (Valenti et al. 1998), characteristic of late spectral types. The best match to standard spectra is between K4V and K5V, just where the TiO absorption bands begin to be noticeable. The comparison K4V and K5V spectra more show pronounced H$\alpha$ absorption, while this line in Gaia21bcv is fainter, and variable in the series of SNIFS medium-resolution spectra. The steep continuum slope is caused by extinction along the line of sight. We have dereddened the combined SNIFS spectra to match the overall continuum slope of a K4-type star, by applying the extinction function of Wang & Chen (2019) with $A_V = 3.2$. The mean wavelength of the Gaia $G$ bandpass is 639.74 nm (Weiler 2018), for which the Wang & Chen (2019) extinction is $A_G = 0.80$ $A_V = 2.56$. As confirmation of this extinction estimate, Gaia DR3 has $B_p - R_p = 2.59$ for this star. The Bayestar19 (Pan-STARRS-based) reddening is $E(B − V) \sim 1.0$, consistent with the extinction value from the spectral slope.

In the top panel in Figure 3, the bright-phase photometry of Gaia21bcv is fitted with a blackbody of $T = 4500$ K and $A_V = 3.2$ (red). To indicate the uncertainty of this combination,
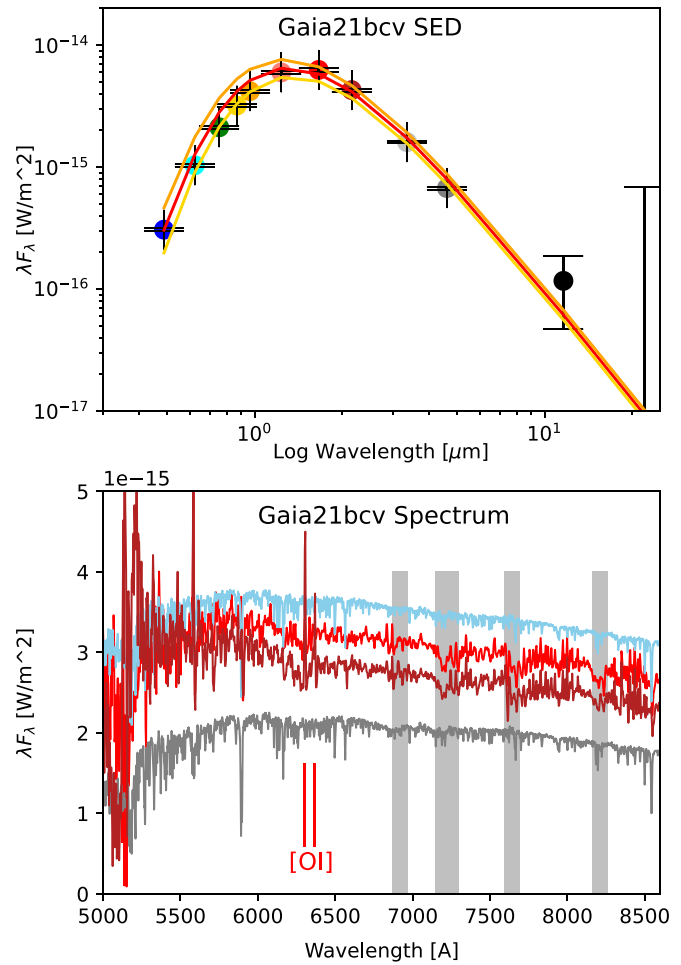




**Figure 3.** The top panel shows the photometry of Gaia21bcv in unobscured condition, fitted with a blackbody of $T = 4400$ K and $A_V = 3.2$ (green) or, to indicate the uncertainty of this combination, $T = 4600$ K and $A_V = 3.6$. Only the WISE3 data point is substantially above this fit, indicating the presence of warm dust. The second panel shows the combined SNIFS spectra before (brown) and after (red) the onset of [O I] emission, dereddened with $A_V = 3.2$. The flux-calibrated spectra of K3V (light blue) and K5V (gray) are shown for comparison and were the basis for the spectral classification of Gaia21bcv.

$T = 4600$ K and $A_V = 3.0$ is indicated in orange and $T = 4400$ K and $A_V = 3.4$ in gold. As confirmation of our spectroscopic determination of the effective temperature, the Gaia DR3 catalog lists the effective temperature as 4520 K, corresponding to a spectral type between K4V and K5V in the tables[11] by Pecaut & Mamajek (2013). We adopt a spectral type of K4.5V for Gaia21bcv in the following discussion. The radius of a K4.5V zero-age main-sequence (ZAMS) star is 0.707 $R_\odot$, interpolated from the same tables.

In the bright phase, the $K_s$ magnitude of Gaia21bcv in the 2MASS Catalog is 13.338. The extinction of $A_V = 3.2$ corresponds to $A_{Ks} = 0.238$ (Wang & Chen 2019). With a distance of 1382 pc and a distance modulus of 10.70, Gaia21bcv has an extinction-corrected absolute magnitude of $M_{Ks} = 2.40$. With the absolute magnitude and colors from the tables of Pecaut & Mamajek (2013) a K4.5V star has $M_{Ks} = 4.32$, making Gaia21bcv 1.92 mag (a factor of 5.86) brighter than the main sequence and the radius 2.42 times larger, i.e., Gaia21bcv has a radius of 1.7 $R_\odot$. The spectral
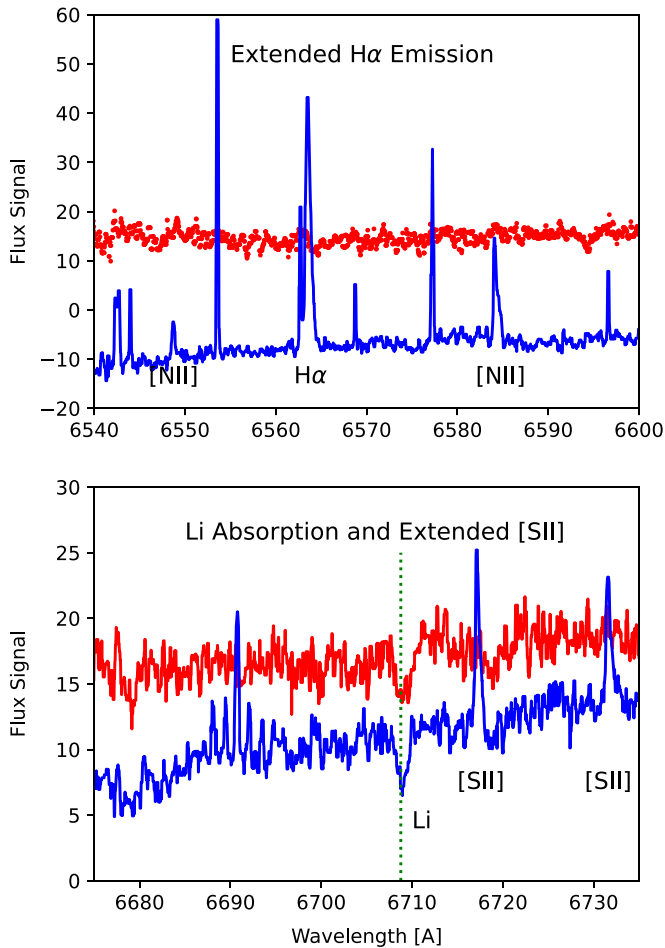
---

[11] http://www.pas.rochester.edu/~emamajek/

**Figure 4.** The two panels are small sections of the Keck HIRES spectrum of Gaia21bcv in stable bright condition, showing absorption and Hα and [N II] extended emission (top) and Li I absorption in the star (bottom). The top panel displays the spectrum without sky subtraction in blue and shows the broad Hα and [N II] lines near Gaia21bcv and, of course, many narrow telluric night sky emission lines. The sky-subtracted spectrum (red, in different flux scaling for clarity) displays the spectrum of the star itself and does not show any noticeable Hα absorption or emission. The bottom panel similarly displays the sky-subtracted spectrum of Gaia21bcv in red and the spectrum of the extended emission plus the star in blue. Both spectra show the Li I absorption line in the star. The blue spectrum without sky subtraction shows the [S II] doublet in emission.

energy distribution (SED) from PS1, 2MASS, and WISE data points can be fitted well with a blackbody of $T = 4500$ K and extinction of $A_V = 3.2$ mag and the (Wang & Chen 2019) extinction law. Integration of this blackbody fit over the wavelength range gives a luminosity of 4.3 $L_\odot$. Both arguments clearly indicate that Gaia21bcv is overluminous compared to the ZAMS and therefore a pre-main-sequence star.

The long-slit Keck HIRES spectrum in Figure 4 shows the Hα and [N II] emission that permeates the region near Gaia21bcv (blue spectrum), but net emission at the position of the star in the sky-subtracted spectrum is not detected (red spectrum). This is consistent with the finding by Pettersson & Reipurth (2019) in their objective prism search for Hα emission stars in the CMa OB1/R1 region that Gaia21bcv was not included in their list of Hα emitters.

The extended Hα emission away from the star has two components: a narrow telluric component and the broader component originating in the nebulosity near Gaia21bcv. This emission is redshifted by 38 km s$^{-1}$ relative to the telluric

emission. A Gaussian fit to its profile gives $\sigma = 11$ km s$^{-1}$. The radial velocity of the star Gaia21bcv of 31 km s$^{-1}$ is therefore well within the velocity dispersion of the Hα emission line. This is consistent with the star being physically located within this H II emission region. Based on this limited information, we conclude that Gaia21bcv has the characteristics of a weak-line Class III pre-main-sequence star with a K4–5 photosphere and variable line emission.

### 3.2.2. Lithium Absorption

The Keck HIRES spectrum of Gaia21bcv shows strong absorption in the Li 6708 Å line, stronger than the Ca I line at 6717 Å. The equivalent width of the Li 6708 Å absorption line is $334 \pm 40$ mÅ. In stars with strongly convective atmospheres, i.e., spectral classes K and M, lithium is destroyed over a timescale of order $10^8$ yr. As specific examples, in the K dwarfs in the $\approx 600$ Myr old Hyades cluster, Soderblom et al. (1995) did not detect any Li absorption. The younger $\approx 70$ Myr old (Soderblom et al. 1995) Pleiades cluster shows Li absorption in K-type stars (Jones et al. 1996), with equivalent widths between 30 and 300 mÅ. In the young, about $5\ 10^6$ year old, cluster NGC 2264, Bouvier et al. (2016) found strong Li absorption in K-type stars, with some dependence of the line equivalent width on the rotation period. In this young cluster, the Li equivalent widths lie between 500 and 550 mÅ. The line observed in Gaia21bcv lies just above the distribution of equivalent width for K-type stars in the Pleiades, and is about half of the typical value in NGC 2264. This suggests an age for Gaia21bcv between those two cases, and probably closer to that of the Pleiades. As an estimate, we adopt the rounded average age of these two clusters, $40 \pm 10$ Myr for Gaia21bcv.

The widths of the absorption lines of the Na I doublets, the strongest absorption lines in the spectrum, were measured. Under the simplistic assumption that vsini $\leqslant$ FWHM/2, we get vsini $\leqslant$ 13 km s$^{-1}$. Compared to the rotational velocities measured by Jones et al. (1996) in the Pleiades, Gaia21bcv is thus a relatively slow rotator, which correlates with the lower abundance of lithium, as first pointed out by Butler et al. (1987).

### 3.2.3. Emission Lines

The SNIFS spectra can be divided into two groups: those taken up to MJD 59638 (2022 February 28) without [O I] emission, and those taken in the 10 days period after MJD 59653 (2022 March 15) up to MJD 59663 (2022 March 25) that show prominent emission of the [O I] doublet. The onset of this emission, happening about 100 days after the end of the last dipping event, is apparently not connected to the end of these dipping events, but may be caused by independent variations in weak accretion that happen in the innermost regions of a circumstellar disk.

We note that the comparison of the averaged SNIFS spectra with and without [O I] also shows varying Hα absorption. We conclude that the Hα absorption of the stellar photosphere is mostly filled in by time-variable chromospheric emission.

On the other hand, the lack of strong and numerous emission lines—e.g., Hα, the Ca II IR triplet, and Na I—that are often observed in classical T Tauri stars rules out strong accretion in this object, and any explanation that the dips were caused by absorption from accretion funnels (Bessolaz et al. 2008), which have been used to explain dipping events in T Tauri stars (Pouilly et al. 2021).
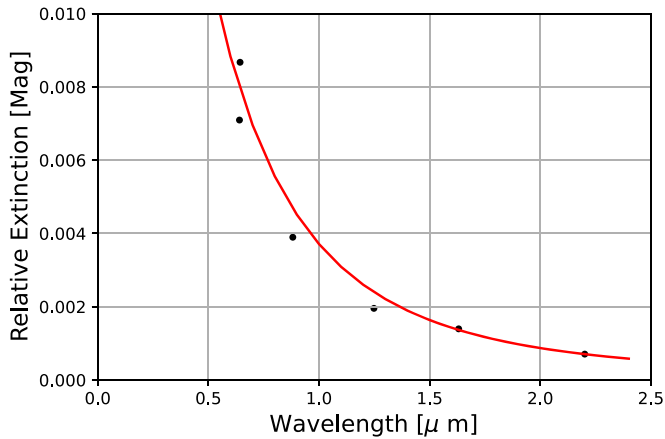
**Figure 5.** The extinction in the last 40 days of the dipping episode has a wavelength dependence closely resembling interstellar extinction.

### 3.3. Wavelength Dependence of Absorption

The monitoring campaign initiated in the late 2021 visibility period of Gaia21bcv was intended to obtain multiwavelength photometry of the light curve. As it turned out, only the first ≈40 days, from MJD 59480 to 59520, recorded the end of the last dipping event in this recent episode. We work under the assumption that the dipping episode is caused by absorption by dust, obscuring the star Gaia21bcv. Therefore, the multi-wavelength light curves give some information about the wavelength dependence of the dust absorption. In each of the filters, we computed the slope of a linear regression approximation of the light curve (in magnitudes) in the 40 days time interval. This slope is proportional to the extinction, and Figure 5 shows the slope value compared to the extinction law (Wang & Chen 2019), normalized to match the measured value in the UKIRT $K$ band. The wavelength dependence of the light-curve slope at the end of the dipping episode closely matches the wavelength dependence of the interstellar extinction on which the Wang & Chen (2019) law is based. This indicates that the dust in the obscuring material contains particles smaller than the wavelength of the observations and similar in size distribution to the interstellar medium.

### 3.4. IR (WISE) Light Curve

The NEOWISE data confirm that Gaia21bcv was of constant brightness prior to MJD 58600. Four NEOWISE data points were obtained during the dipping episode, during which the W1–W2 color was positive (i.e., redder), in contrast to the constant bright phase when the W1–W2 color was neutral. The two data points near the middle of the dipping episode are fainter than the quiescent brightness, and the other two are brighter. The brightest W1 and W2 magnitudes were observed within days of the deepest observed optical dip.

The data points in the stable bright phase, i.e., MJD ⩽ 58406 and MJD ⩾ 59659, have average W1 = 13.135 ± 0.031 (SD) and W2 = 13.074 ± 0.050 (SD), and thus W1–W2 = 0.061 ± 0.016 (standard error of the mean). The $A_V =$ 3.2 mag interstellar extinction of Gai21bcv gives an $E$(W1–W2) = −0.042, using the extinction law by Wang & Chen (2019). In the list of Pecaut & Mamajek (2013), stars in the age range 5–30 Myr of K4 spectral type have neutral W1–W2 = 0.00 mag color. The observed W1–W2 = 0.06 ± 0.02 in

the stable bright phase is therefore consistent with a pre-main-sequence K4 star with $A_V$ = 3.2.

During the dipping phase, which we interpret as the result of occultation by some form of dust cloud, we have four NEOWISE data points (Table 1 and Figure 1). The two data points at the beginning and end of the occultations are below the stable brightness, while the two data points in the middle of the occultation phase are brighter than the unobscured brightness. During this phase, the W1–W2 color is redder at all the four epochs recorded than during the unobscured phase.

## 4. Discussion

For most of the time that we have observations of, Gaia21bcv is of near-constant brightness within the errors of our photometry. The light curve in Figure 1 shows a distinct episode of several deep and sharp minima. The beginning and the end of this episode are equally well defined, and we do not see evidence for any gradual clearing of the obscuration. We base this discussion on the assumption that the star is of constant observed brightness most of the time and that the episode of dipping events events represents a rare occurrence.

Based on the wavelength dependence of the absorption (Figure 1, bottom panel, and Figure 5) during the minima, we conclude the dipping events are due to occultations of the star by dust that contains at least some small particles. We will discuss the nature, spatial structure, and distance of that dust in the following discussion.

### 4.1. Is Gaia21bcv an RCB Star?

The light curve of Gaia21bcv has similarities to that of some RCB variables, reviewed by Clayton (1996). In those old, carbon-rich AGB supergiants, the episodic formation of carbon dust clouds in the variable wind emerging from the star leads to episodic, irregular minima lasting months to years that bear a superficial resemblance to those observed in Gaia21bcv. For a direct comparison, the prototypical R CrB at a distance of 696 pc and neglecting extinction, has $M_{KS}$ = −4.65 mag at least, and is therefore clearly in a different luminosity class from Gaia21bcv. Most RCB stars have spectral types of F and G (Clayton 1996), and their optical spectra show the molecular $C_2$ Swan bands in absorption, characterizing these stars as extremely overabundant in carbon. The SNIFS spectra of Gaia21bcv show no indication of $C_2$ absorption and are not consistent with an RCB star. While Gaia21bcv is above the main-sequence absolute magnitude, it is far below the luminosity and absolute V magnitude of R CrB. Its relatively low-luminosity, $C_2$-free spectrum, and its apparent association with star formation in its vicinity, are the strongest arguments that Gaia21bcv is, in fact, not an RCB variable.

It should be noted that the clear detection of Li I absorption at nominally 6708 Å does not strengthen the case against being an RCB star, since Li can be produced in the He flash forming the RCB star (Clayton et al. 2011). However, since the RCB explanation is excluded, based on the absolute magnitude and lack of $C_2$ absorption, the Li absorption provides additional evidence that Gaia21bcv is indeed a young object, independent of the circumstantial evidence from the Hα emission, dark clouds, and IRAS sources in its vicinity. Main-sequence stars with spectral types K and M show very little lithium absorption, as has already been pointed out by Herbig (1965), due to the deep convection in their atmospheres during

their contraction phase and also in their early-main-sequence phase that leads to the rapid destruction of Li. The detection of Li in Gaia21bcv with its late spectral type is therefore another strong indication of a very young star.

### 4.2. Occultation by an Orbiting Object

Many young stars show the "dipping" behavior, i.e., multiple, repeated short dips in brightness. The most common dipper objects are very young, still-accreting classical T Tauri stars, of which up to 25% show dipper-like variability. For these accreting stars, Ansdell et al. (2016) have shown a correlation between dipping depth and IR excess, i.e., the more warm dust is present in the immediate vicinity of the star, the deeper the dips in brightness are. However, in Gaia21bcv, we do not observe substantial excess emission at 4.6 $\mu$m in the bright-phase SED and the bright phase W1–W2 color is, within the errors, as expected for a K4–5 pre-main-sequence star with $A_V = 3.2$ mag foreground interstellar extinction. The deep occultation events and, at the same time, little IR excess at near to mid-IR wavelengths support what is already strongly suggested by the episodic nature of the occultations and long intervals between these episodes: the obscuring dust is concentrated on a small section of the orbit, the overall mass of dust around the star is small, and the distance of the dust from the star is so large that, due to the combination of these factors, IR excess is not observed at short and mid-IR wavelengths. Such a dust cloud at substantial distance from the star could have been produced by a catastrophic collision of two small planetesimals or asteroids. Such events have indeed been observed by an increase in IR emission, which is approximately isotropic and can be observed from any direction, making the discovery of such spikes in IR emission likely. Results for two objects, ID8 and P1121, have been summarized by Su et al. (2019). In both objects, the orbital periods, collisional cascade buildup time of the dust cloud, and cloud dispersal times are of the order of years.

In at least one case, a recently produced dust cloud has been directly imaged: Formalhaut b, initially thought to be an exoplanet, was found by Gaspar & Rieke (2020) to be an expanding, very-low-mass cloud of debris, after what appears to have been an asteroid collision. Based on measurements of the cloud expansion, they estimate that the cloud had formed only a few years prior to its discovery and is dissipating on timescales of a few decades. The dissipation time depends, of course, on the initial velocity of the collision debris.

By comparison, the occulting object around Gaia21bcv is larger and more opaque, but without a massive object, it would probably still dissipate on timescales of decades or centuries. While we cannot categorically exclude the possibility of a short-lived dust cloud, it would be a very unlikely event to find such a short-lived object at large distances from its host star in just the right orientation toward the observer to appear transiting in front of the star.

Frequent, sporadic, short, and comparatively shallow dips in the light curve of the main-sequence star KIC 8462852 were discovered by Boyajian et al. (2016). The best explanation for these short dipping events is swarms of comets briefly obscuring the star. However, the much longer and deeper brightness minima of Gaia21bcv are much more substantial than what could be explained with anything close to comets in our own solar system.

In addition, the occulting object in Gaia21bcv appears to be well defined, with no indications of a gradual temporal clearing or smooth profile of the dipping events in the light curve. The light curve does, instead, suggest a well-defined outer edge of a disk or a ring system.

We therefore favor a model, similar to $\epsilon$ Aur, of a long-lasting disk or ring system, where the containment of the dust or debris cloud along its orbital path must be aided by the presence of a companion body of dynamically significant mass.

### 4.3. Absorption and Scattering

In the case of Gaia21bcv, the only available data in the mid-IR are from the WISE/NEOWISE (Wright et al. 2010; Mainzer et al. 2014) mission. The WISE W3 band shows a faint, $4.7\sigma$ detection. The WISE W4 image shows a $2\sigma$ source that is extended and includes the position of Gaia21bcv. Based on the same WISE data, Gregorio-Hetem et al. (2021) have classified Gaia21bcv as a Class III object, i.e., a pre-main-sequence star without significant IR excess.

While the W1–W2 colors are nearly neutral (zero) in the bright phase, during the dipping episode, the color was redder (W2 brighter). There are two possible explanations, not necessarily mutually exclusive, for this change in mid-IR colors: first, all dust size distributions containing particles much smaller than the wavelength observed tend to absorb stronger at shorter wavelengths and second, additional flux at longer wavelengths would change the color. We have measured the color dependence of the dust absorption in the last few weeks of the occultation phase, and confirmed a wavelength dependence similar to that of the interstellar medium, specifically the extinction law by Wang & Chen (2019). In addition and somewhat surprisingly, two of the NEOWISE IR data points during the occultation phase are above the unobscured brightness, indicating the addition of mid-IR flux near the middle of this phase.

Any additional thermal emission from the obscuring cloud would be radiated isotropically and would be observable in all phases of the cloud's orbit. We do not observe any fluctuations of the W1 or W2 flux in the unobscured bright phase and, therefore, increases in thermal emission must be very rare. The sudden addition of thermal emission just in the middle of the occultation phase would be purely coincidental and very unlikely. We therefore suggest that the IR flux during the occultation is the superposition of two opposite effects: enhanced flux due to forward scattering in the dust cloud and, of course, absorption by this same dust. At the optical wavelengths where most of data were obtained, absorption dominates and no data point during that phase exceeds the unobscured flux. At the WISE W1 and W2 wavelengths, absorption is present and leads to a reddening of the observed color in all four data points, and the minima at two epochs, but forward scattering directs so much additional flux toward the observer that the center two data points actually exceed the unobstructed brightness level.

Strong forward scattering has been observed in the more tenuous rings of the Saturn ring system and discussed by Hedman & Stark (2015) as a possible analog to the dust in debris disks around other stars. Even earlier in the evolution of dust particles, strong scattering at IR wavelengths is evident in the core shine phenomenon observed in isolated small molecular clouds illuminated by the interstellar radiation field (Steinacker et al. 2015). A detailed analysis or modeling of the
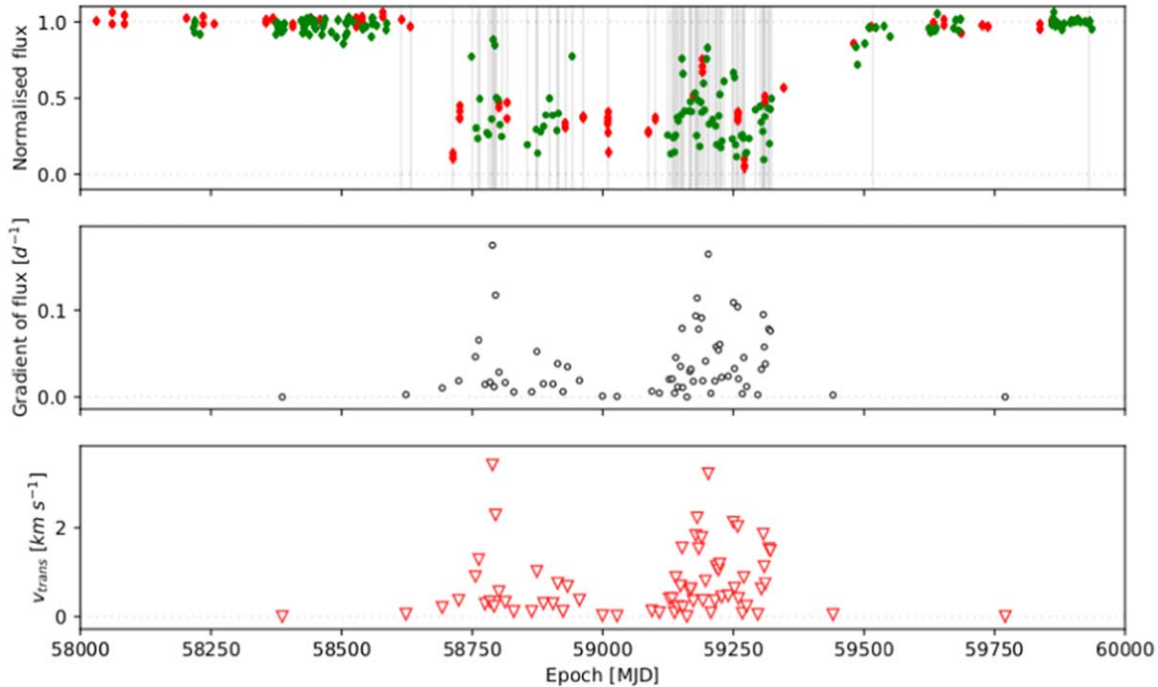
**Figure 6.** Analysis of the light-curve gradients as a velocity of the obscuring object with the exoring analysis procedure. The analysis indicates a lower limit to the transverse velocity of 2 km s$^{-1}$. This slow transverse velocity indicates a large orbital radius and period for the obscuring objects, of order 30 au. The upper panel shows the normalized flux light curve of the star. The gray vertical lines mark the boundaries of sections where the light curve is linearly increasing or decreasing. The middle panel shows the measured light-curve gradient as a function of time for the eclipse. The lower panel shows the derived transverse velocity, assuming the given radius of the star quoted in the text. Error bars are shown at $1\sigma$ confidence.

dust properties in the Gaia21bcv occulting disk is beyond the scope of this paper, but based on the properties of both the younger and older dust mixtures mentioned above, strong forward scattering in the occulting disk is a plausible scenario.

### 4.4. A Transiting Ring System

The model of an orbiting dust cloud, held together by some massive body, is conceptually similar to the now well-established model for the periodic deep minima of $\epsilon$ Aurigae, summarized by Hoard et al. (2010). In this model of $\epsilon$ Aurigae, a dense dust cloud orbiting a companion star occults the primary star periodically, but that companion is not itself visible at optical wavelengths. In contrast to $\epsilon$ Aurigae, the occultation event in Gaia21bcv is not simply a smooth minimum, but a series of sharp minima between brighter periods that in some cases return almost to the unoccluted brightness. This indicates more structure in the orbiting dust cloud than is observed in $\epsilon$ Aurigae. For an eclipse by a disk with substructure—for example, a ring system—the modulation by the orbital motion in front of the star is dominant over temporal variations in the cloud for plausible combinations of the orbital period, size of the dust cloud, and rotation of the dust cloud.

Mamajek et al. (2012) specifically apply this model of a highly structured disk around an orbiting companion object, possibly a ring system, to the case of SWASP J140747.93-394542.6, where multiple deep minima spread over ≈54 days were observed.

Their preliminary model was refined further by van Werkhoven et al. (2014) and Kenworthy & Mamajek (2015), who fit their light curve with an elaborate model of an eclipse by a multiple ring system around a planetary companion.

Similarly and even earlier, Mikolajewski & Graczyk (1999) have discussed the case of EE Cep, where multiple, long-duration minima have been observed, interpreted as eclipses by an optically thick disk around a companion object.

We have no evidence from the high-resolution spectrum of line splitting and therefore the presence of a stellar companion. Gaia21bcv is listed in Gaia EDR3 with a RUWE of 1.06, indicating a solid detection, with no evidence of astrometric wobble that might indicate an orbiting companion. We can only speculate that the companion object stabilizing the dust cloud may be an otherwise unobservable companion of stellar, substellar, or planetary mass.

We determined an estimate of the transverse velocity of the dust by analysis of the gradients in the light curve of the star. We followed the "exoring" prescription in van Werkhoven et al. (2014), where we obtain an upper bound on the transverse velocity by assuming that each of the individual flux dips is caused by an opaque occulter much larger than the diameter of the star that it is transiting. When the edge of the occulter is perpendicular to the direction of motion, this enables an upper estimate of the transverse velocity of the cloud, since an edge that is not perpendicular to the vector of motion will require a higher velocity to cover the entire disk of the star.

The method is as follows: the light curve is converted from stellar magnitudes to flux, and the flux light curve is divided by the "out of eclipse" flux level to produce a normalized flux curve (see the upper panel of Figure 6). The light curve is visually inspected to identify turning points (indicated by the gray vertical lines in the upper panel), which we associate with a new edge with different opacity beginning to transit the stellar disk. A straight line is then fit to the photometry between these turning points, and a gradient with an associated measurement error is determined—this is plotted in the middle panel of

Figure 6. Together with the diameter of the star, a lower bound on the transverse velocity of the material can be determined. Assuming a radius of $1.7R_\odot$ for the star, the transverse velocity is shown in the lower panel of Figure 6.

The analysis showed a robust lower speed of 2 km s$^{-1}$ for the occulter. This lower limit is partly due to the limited sampling of the light curve during the major minima, before the dedicated high-cadence monitoring was initiated. Multiplying the velocity by the duration of the eclipse gives a lower estimate for the diameter of the occulter. For an eclipse duration of 866 days and a velocity of 2 km s$^{-1}$, the estimated diameter of the eclipsing disk is 1.0 au. The 866 days duration includes a minor gradient before the first observed deep minimum and establishes a more symmetric light curve. The distribution of the gradients as a function of time shows approximate time symmetry, with a notable dip in the measured gradients at the approximate midpoint of the eclipse. Using the analysis of light-curve gradients as a function of time as described in Kenworthy & Mamajek (2015), this is qualitatively consistent with a disk with azimuthally symmetric substructure that is moderately inclined and the projected semimajor axis of the ring system is close to being parallel with respect to the path of the star behind the rings. Assuming, for an order of magnitude estimate, that Gaia21bcv has a mass of $1\,M_\odot$, an orbital velocity of 2 km s$^{-1}$ implies a radius of a circular orbit of 225 au and an orbital period of 3375 yr. Since the orbital velocity is a lower limit, these estimates for radius and orbital period are upper limits. Even with this caveat, repeat observations of a second transit are a very distant prospect.

### 4.5. Is an Orbiting Disk Consistent with the Age ?

The SED of Gaia21bcv outside of the occultation events is essentially a reddened photosphere, with only minimal indication of a possible IR excess in the W3 filter, leading to the classification of Gaia21bcv as a Class III star whose protostellar disk has largely dispersed. While there is a large scatter in the disk clearing times for individual stars, reviewed by Williams & Cieza (2011), its Class III properties suggest an age of at least 10 Myr for Gaia21bcv. Together with the membership in an OB association and its pre-main-sequence luminosity, all this points to Gaia21bcv having an age in the range of 10–40 Myr. It is therefore plausible that at an age when the protoplanetary disk around the primary star Gaia21bcv has largely dissipated, a smaller (only 1 au) disk at a substantial distance from the primary star, orbiting a secondary, less massive component, has escaped disk clearing and may still persist. While it appears clear that a massive body is needed to keep that occulting disk together, this object appears to be invisible and we cannot constrain its mass. Anything from a low-mass star, a future brown dwarf, or a young giant planet would be possible. It may be possible to observe the thermal emission from the occulting disk, to place constraints on its internal heating by the secondary object and thereby on the luminosity of that object.

### 5. Summary and Conclusions

Gaia21bcv has undergone an episode of repetitive, deep minima in its brightness between 2019 August 18 (MJD 58713) and 2021 November 2 (MJD 59520), after showing constant brightness before and after this dipping episode. The star is a young, probably still weakly accreting pre-main-sequence star and most likely a member of the CMa OB1/R1 association. The star is approximately of K4–5 spectral type with strong metal absorption lines, including Li absorption that indicates its youth. H$\alpha$ was weakly detected in absorption and was variable. Variable [O I] emission was detected after the end of the dipping episode and extended [S II] was detected, both indicating shock-excited gas.

The dipping episode can be understood in a model similar to that of $\epsilon$ Aurigae: Occultation by a large dust cloud orbiting the primary star. The dust cloud is probably surrounding a star or planet sufficiently massive to prevents is rapid dissipation. In contrast to $\epsilon$ Aurigae, the occultation minimum is not as stable but consists of multiple dipping events, suggesting a more clumpy distribution of the dusty material or a system of rings. We suggest that the occulting object may be a circumstellar or circumplanetary debris disk around an otherwise undetected companion object to Gaia21bcv.

## ORCID iDs

Klaus W. Hodapp ● https://orcid.org/0000-0003-0786-2140
Eric Gaidos ● https://orcid.org/0000-0002-5258-6846
Matthew A. Kenworthy ● https://orcid.org/0000-0002-7064-8270
Michael Tucker ● https://orcid.org/0000-0002-2471-8442
Benjamin J. Shappee ● https://orcid.org/0000-0003-4631-1149
Anna V. Payne ● https://orcid.org/0000-0003-3490-3243
Aaron Do ● https://orcid.org/0000-0003-3429-7845

## References

Ansdell, M., Gaidos, E., Rappaport, S. A., et al. 2016, ApJ, 816, 69
Bellm, E. C., Kulkarni, S. R., Graham, M. J., et al. 2019, PASP, 131, 018002
Bessolaz, N., Zanni, C., Ferreira, J., et al. 2008, A&A, 478, 155
Bouvier, J., Lanzafame, A. C., Venuti, L., et al. 2016, A&A, 590, A78
Boyajian, T. S., LaCourse, D. M., Rappaport, S. A., et al. 2016, MNRAS, 457, 3988
Brown, T. M., Baliber, N., Bianco, F. B., et al. 2013, PASP, 125, 1031
Butler, R. P., Cohen, R. D., Duncan, D. K., et al. 1987, ApJL, 319, L19
Casali, M., Adamson, A., Alves de Oliveira, C., et al. 2007, A&A, 467, 777
Clayton, G. C. 1996, PASP, 108, 225
Clayton, G. C., Sugerman, B. E. K., Stanford, S. A., et al. 2011, ApJ, 743, 44
Dobashi, K. 2011, PASJ, 63, S1
Flewelling, H. A., Magnier, E. A., Chambers, K. C., et al. 2020, ApJS, 251, 7
Gaia Collaboration, Prusti, T., de Bruijne, J. H. J., et al. 2016, A&A, 595, A1
Gaia Collaboration, Vallenari, A., Brown, A. G. A., Prusti, T., et al. 2023, A&A, 674, A1
Gaidos, E., Mann, A. W., Rojas-Ayala, B., et al. 2022, MNRAS, 514, 1386
Gaspar, A., & Rieke, G. 2020, PNAS, 117, 9712
Gregorio-Hetem, J., Lefloch, B., Hetem, A., et al. 2021, A&A, 654, A150

Hedman, M. M., & Stark, C. C. 2015, ApJ, 811, 67
Herbig, G. H. 1962, AdA&A, 1, 47
Herbig, G. H. 1965, ApJ, 141, 588
Herbst, W., Herbst, D. K., Grossman, E. J., et al. 1994, AJ, 108, 1906
Hoard, D. W., Howell, S. B., & Stencel, R. E. 2010, ApJ, 714, 549
Hodgkin, S. T., Irwin, M. J., Hewett, P. C., et al. 2009, MNRAS, 394, 675
Jones, B. F., Shetrone, M., Fischer, D., et al. 1996, AJ, 112, 186
Kearns, K. E., & Herbst, W. 1998, AJ, 116, 261
Kenworthy, M. A., & Mamajek, E. E. 2015, ApJ, 800, 126
Lawrence, A., et al. 2007, MNRAS, 379, 1599
Mainzer, A., Bauer, J., Cutri, R. M., et al. 2014, ApJ, 792, 30
Mamajek, E. E., Quillen, A. C., Pecaut, M. J., et al. 2012, AJ, 143, 72
Masci, F. J., Laher, R. R., Rusholme, B., et al. 2019, PASP, 131, 018003
McCully, C., Volgenau, N. H., Harbeck, D.-R., et al. 2018, Proc. SPIE, 10707, 107070K
Mikolajewski, M., & Graczyk, D. 1999, MNRAS, 303, 521
Pecaut, M. J., & Mamajek, E. E. 2013, ApJS, 208, 9
Pettersson, B., & Reipurth, B. 2019, A&A, 630, A90
Pouilly, K., Bouvier, J., Alecian, E., et al. 2021, A&A, 656, A50
Roggero, N., Bouvier, J., Rebull, L. M., et al. 2021, A&A, 651, A44
Santos-Silva, T., Perottoni, H. D., Almeida-Fernandes, F., et al. 2021, MNRAS, 508, 1033
Skrutskie, M. F., Cutri, R. M., Stiening, R., et al. 2006, AJ, 131, 1163
Soderblom, D. R., Jones, B. F., Stauffer, J. R., et al. 1995, AJ, 110, 729
Steinacker, J., Andersen, M., Thi, W.-F., et al. 2015, A&A, 582, A70
Su, K. Y. L., Jackson, A. P., Gáspár, A., et al. 2019, AJ, 157, 202
Tucker, M. A., Shappee, B. J., Huber, M. E., et al. 2022, PASP, 134, 124502
Valenti, J. A., Piskunov, N., & Johns-Krull, C. M. 1998, ApJ, 498, 851
van Werkhoven, T. I. M., Kenworthy, M. A., & Mamajek, E. E. 2014, MNRAS, 441, 2845
Vogt, S. S., Allen, S. L., Bigelow, B. C., et al. 1994, Proc. SPIE, 2198, 362
Wang, S., & Chen, X. 2019, ApJ, 877, 116
Weiler, M. 2018, A&A, 617, A138
Williams, J. P., & Cieza, L. A. 2011, ARA&A, 49, 67
WISE Team 2020, NEOWISE 2-Band Post-Cryo Single Exposure (L1b) Source Table IPAC, https://irsa.ipac.caltech.edu/cgi-bin/Gator/nph-dd?catalog=allsky_2band_p1bs_psd
Wood-Vasey, W. M., Aldering, G., Lee, B. C., et al. 2004, NewAR, 48, 637
Wright, E. L., Eisenhardt, P. R. M., Mainzer, A. K., et al. 2010, AJ, 140, 1868